Van der Waals density functional study of *n*-alkane adsorbed on metal surfaces

Yuji Hamamoto,[1,*] Takanori Shimada,[1] Tomohiro Kimura,[1] Kouji Inagaki,[1] Ikutaro Hamada,[1] and Yoshitada Morikawa[1,2]

[1]*Department of Precision Engineering, Graduate School of Engineering, Osaka University, Suita, Osaka 565-0871, Japan*
[2]*Research Center for Precision Engineering, Graduate School of Engineering, Osaka University, Suita, Osaka 565-0871, Japan*

We present a comprehensive study of *n*-alkane adsorbed on metal surfaces using the van der Waals density functional (vdW-DF) method. This method outperforms the density functional theory calculations within the local density or generalized gradient approximation in terms of a better description of a wide range of physisorption systems. Especially, our results demonstrate that vdW-DFs with improved accuracy nicely predict the adsorption heights of *n*-alkanes on close-packed metal surfaces. We also show that the C–H stretching frequencies and infrared absorption spectra are useful for discriminating the competing adsorption structures. Detailed analyses of the properties of *n*-alkanes on metal surfaces, however, reveal some discrepancies with experimental results, suggesting that further improvement of vdW-DF or the application of a more sophisticated technique is necessary for a systematic description of the *n*-alkane-metal interfaces with higher accuracy.

I. INTRODUCTION

A detailed understanding of the interfaces between organic molecules and metal electrodes is crucial for developing high-performance organic devices. For example, the electric dipole layer formed at an organic-metal interface influences the charge injection barrier [1]. Among the mechanisms proposed as the origin of the interface dipole layer, the push back effect due to the Pauli repulsion [2, 3] plays an essential role in the adsorption of inert and nonpolar organic molecules such as *n*-alkanes. Although *n*-alkanes adsorbed on metal surfaces appear to be typical physisorption systems, experiments have revealed that the C–H bonds are significantly softened at the interfaces [4–12], suggesting that these systems bear the character of weak chemisorption.

To elucidate the properties of *n*-alkanes on metal surfaces, a variety of experimental techniques have been employed such as infrared reflection absorption spectroscopy (IRAS) [4–11, 13–21], low energy electron diffraction (LEED) [10, 11, 22–27], and temperature programmed desorption (TPD) [18, 21, 27–35]. Theoretically, first principles calculations based on density functional theory (DFT) have been applied to *n*-alkanes on metal surfaces, mainly from industrial viewpoints such as the Fischer-Tropsch synthesis [36–44], dehydrogenation of hydrocarbons [45–48], and charge injection barriers [49–51]. DFT calculations have also been used to investigate the geometric and electronic structures of several *n*-alkane-metal interfaces [45, 46, 48, 52–56]. Morikawa *et al*. have studied *n*-alkanes adsorbed on various metal surfaces within the generalized gradient approximation (GGA), demonstrating that DFT calculations can reproduce the vacuum level shift and the softening of C–H stretching modes that have been observed experimentally [52]. However, the GGA results underestimate the adsorption energies of *n*-alkanes, due to the lack of van der Waals (vdW) interactions. In the last two decades, several vdW corrections have been proposed for use in DFT calculations [57–62], among which the vdW density functional (vdW-DF) method [57, 63, 64] is a scheme to describe vdW interactions without semi-empirical parameters. Moreover, new functional forms of vdW-DF have been actively developed until recently [65–75].

In this paper, we apply vdW-DF to the investigation of the adsorption of *n*-alkanes on various metal surfaces. Our results reveal that the rev-vdW-DF2 [71, 76] and optB86b-vdW [69] functionals predict reasonable adsorption energies of *n*-alkanes on the Cu(100) and Cu(111) surfaces, respectively, whereas the two functionals significantly overestimate those on the close-packed surfaces of other metals. In contrast, the adsorption heights of *n*-alkanes on the latter surfaces obtained with the two functionals are in good agreement with those estimated from the vacuum level shift and the softening of the C–H stretching modes. We also show that the changes in the C–H stretching frequencies and IRAS spectra are useful for determining the preference of different adsorption structures of similar stability.

This paper is organized as follows. The details of the DFT calculations used in this work are described in Sec. II. Our calculated results are presented in Sec. III, which consists of three parts: The adsorption structures of *n*-butane on close-packed metal surfaces and those of polyethylene on low-indexed Cu surfaces are determined in Sec. III A. For polyethylene on Cu(100) and (110), the vibrational properties of the molecule are discussed in Sec. III B. The work functions of the above systems are investigated in Sec. III C. This work is summarized in Sec. IV.

II. METHODS

The DFT calculations are carried out using the STATE code [77, 78] with the plane wave basis set. Most of the ion cores are described by ultrasoft pseudopotentials [79], while that of Ag is described by a norm-conserving pseudopotential [80]. The energy cutoffs for wave functions and charge density are 36 and 400 Ry, respectively, except for the systems including Ag, where the cutoff energy for the wave functions is increased to 64 Ry. Metal surfaces are modeled with periodically repeated slabs composed of six atomic layers, where surface reconstruction is not taken into account. The LEED results indicate that *n*-alkane molecules form a close-packed monolayer on Pt(111) at low temperatures with the C–C–C

* Corresponding author: hamamoto@prec.eng.osaka-u.ac.jp

TABLE I. Calculated lattice constants of transition metals in Å. Note that two lattice constants are shown for the hcp structure of Ru.

	rev-vdW-DF2	optB86b-vdW	Experiments[a]
Cu	3.63	3.62	3.61
Ag	4.10	4.09	4.09
Au	4.11	4.14	4.08
Ir	3.85	3.83	3.84
Pt	3.93	3.93	3.92
Ru_a	2.63	2.64	2.70
Ru_c	4.21	4.19	4.28

[a] Reference [94].

plane approximately parallel to the surface [15]. The same trend is also expected for other metals and facets because the molecules are physisorbed on the surface through vdW interactions. Thus, *n*-butane is adsorbed on the (111) surfaces of Cu, Ag, Ir, Pt, and Au, and on the Ru(0001) surface using the ($\sqrt{7} \times \sqrt{3}$) surface unit cell [15], and Γ-centered 4×6 *k* points are sampled in the surface Brillouin zone (SBZ). On the other hand, polyethylene is adsorbed on the Cu(111), (100), and (110) surfaces, using the $(1 \times \sqrt{3})$, (1×2) [23], and (1×4) [11, 23] surface unit cells, respectively. Correspondingly, Γ-centered 12×6, 12×6, and 12×3 *k* points, respectively, are sampled in the SBZs.

The physisorption of the *n*-alkane molecules on the surfaces is described by the self-consistent [63, 81–83] vdW-DF method [57] with the optB86b-vdW [69] and rev-vdW-DF2 [71, 76] functionals. The former is based on the nonlocal correlation functional (E_c^{nl}) of the original vdW-DF [57], while the latter is based on E_c^{nl} of the second version of vdW-DF (vdW-DF2) [54]. vdW-DF employs the gradient expansion for the slowly varying electron gas [84] to describe the internal exchange-correlation energy ϵ_{xc}^{int} for E_c^{nl}, which is responsible for the attractive dispersion force. On the other hand, vdW-DF2 employs the large-*N* asymptote [85, 86] for ϵ_{xc}^{int}, which is more appropriate for molecular systems. vdW-DF predicts more accurate C_6 coefficients than vdW-DF2 [87], but tends to overestimate the attractive interaction due to the dispersion force. optB86b-vdW and rev-vdW-DF2 employ the same enhancement factor of B86b [88] for the exchange functional with different parameterizations, and show similar and consistent results, but the former (latter) tends to predict larger (smaller) adsorption energy and smaller (larger) equilibrium distance, in particular, for weakly interacting systems, as in the case of the present study. See Refs. [89–93] for some benchmark calculations.

The structures of isolated and crystalline *n*-alkane molecules, clean surfaces, and the adsorption systems are relaxed until the atomic forces fall below 8.24×10^{-2} nN (10^{-3} hartree/bohr) except for the bottom three layers of the slabs, which are fixed at the bulk positions with lattice constants as listed in Table I. The zero-point corrections (ZPCs) due to the molecular vibrations are taken into account. The vibrational modes are obtained by diagonalizing the mass-weighted Hessian matrix estimated within the finite-difference approximation [95] as follows. Normal coordinates are roughly estimated by displacing the atoms in the molecules by $\pm 5.29 \times 10^{-3}$ Å ($\pm 10^{-2}$ bohr) in each cartesian direction. Then the accuracy of the vibrational modes is improved by displacing those atoms along the normal coordinates, where the magnitudes of the displacements are chosen in such a way that the maximum force acting on the displaced atoms is $\simeq 2.47 \times 10^{-1}$ nN (3×10^{-3} hartree/bohr). A vacuum layer of 15 Å thick above a metal surface and the effective screening medium method [96, 97] are used to eliminate spurious electrostatic interactions with the periodic images.

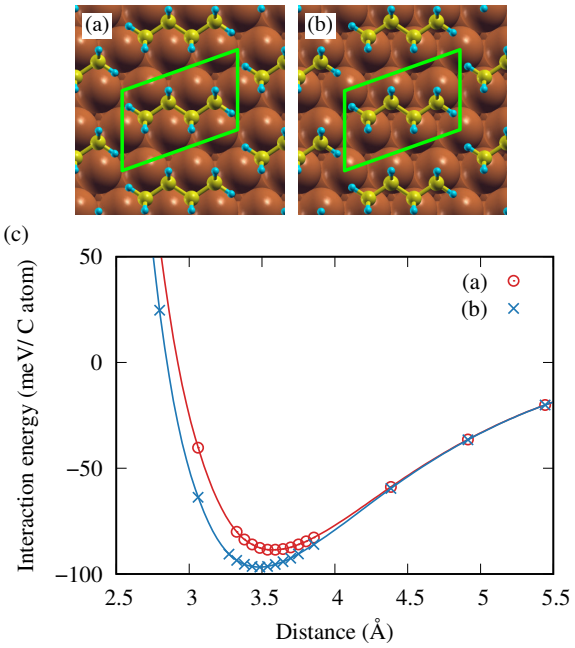

FIG. 1. Schematic views of *n*-butane adsorbed on the Cu(111) surface in two different configurations (a) and (b), where the parallelogram in each panel represents the ($\sqrt{7} \times \sqrt{3}$) unit cell. Panel (c) shows the rev-vdW-DF2 results for the interaction energies between *n*-butane and Cu(111) plotted as functions of the molecule-surface distance.

III. RESULTS

A. Adsorption structures

The determination of the adsorption structures is the first step in studying the properties of the *n*-alkane-metal interfaces. The stabilities of the adsorption structures are compared by using the molecule-surface interaction energy per C atom given by

$$E_{int} = \frac{1}{N_C}(E_{mol/surf} - N_{mol}E_{mol} - E_{surf}). \quad (1)$$

Here E_{mol}, E_{surf}, and $E_{mol/surf}$ are the total energies of an isolated molecule, a clean surface, and their composite system,

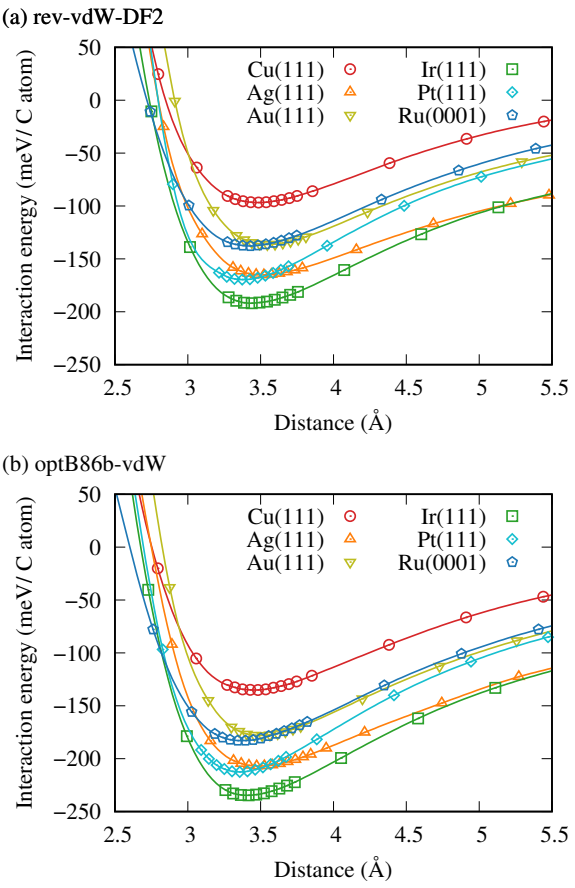

FIG. 2. Interaction energies between *n*-butane and close-packed metal surfaces as functions of the molecule-surface distance. Panel (a) [(b)] show the rev-vdW-DF2 (optB86b-vdW) results for the interaction energies. A *n*-butane molecule is adsorbed on the surface in the configuration shown in Fig. 1(b).

respectively, while N_C and N_{mol} are the numbers of C atoms and molecules, respectively, in a unit cell. In the following, the interaction energy is plotted as a function of the distance between the molecular plane and the metal surface. At each distance, the surface geometry is unchanged, while the molecular structure is relaxed except for the molecular plane, which is kept parallel to the surface.

1. *n-butane adsorbed on close-packed metal surfaces*

To see the dependence of the *n*-alkane-metal interaction on the metal element, we here determine the adsorption structures of *n*-butane on the (111) surfaces of fcc metals and the Ru(0001) surface. Based on the zigzag shape of a *n*-butane molecule and the hexagonal structure of the close-packed surfaces, we examine the two high-symmetry adsorption configurations as shown in Figs. 1(a) and 1(b), which have been considered in Refs. [15] and [52], respectively. The molecular axis is oriented in the $[1\bar{1}0]$ direction in both cases, while C atoms are approximately above the hollow and top sites in the former and latter, respectively. We compare the stabilities of the two configurations by taking *n*-butane on Cu(111) as an example. The interaction energy between *n*-alkane and Cu(111) for rev-vdW-DF2 is plotted as a function of the molecule-surface distance in Fig. 1(c), which indicates that the configuration in Fig. 1(b) is more preferable.

We thus determine the adsorption structures of *n*-butane on the close-packed metal surfaces assuming the adsorption configuration in Fig. 1(b). The interaction energy of *n*-butane on each surface is plotted as a function of the molecule-surface distance in Fig. 2. The rev-vdW-DF2 and optB86-vdW results show qualitatively similar behaviors, but the latter have systematically deeper minima at smaller molecule-surface distances, which agrees with the general trends of these functionals as mentioned in Sec. II. The origin of these differences is discussed in Sec. II of the Supplementary Material [100]. The adsorption structure of each system is determined by fully relaxing the structure near the minimum. The adsorption energy is given by $|E_{int}|$ of the relaxed structure, while the adsorption distance is defined as the average distance between the C atoms in the molecule and the metal atoms in the topmost layer. The calculated adsorption energies and heights are summarized in Tables II and III, respectively. In the former, the

TABLE II. Calculated adsorption energies per C atom of *n*-butane (polyethylene) on the close-packed metal [low-indexed Cu] surfaces in meV. The adsorption energies without ZPC are shown in parentheses. The experimental results are obtained for *n*-butane adsorbed on the metal surfaces.

System	rev-vdW-DF2	optB86b-vdW	Experiments
n-butane			
Cu(111)	113 (100)	134 (129)	127[a]
Ag(111)	207 (166)	227 (207)	···
Au(111)	165 (138)	193 (177)	105[b]
Ir(111)	219 (192)	256 (235)	···
Pt(111)	202 (171)	233 (210)	120[a]
			131[c]
			132[d]
			156[e]
Ru(0001)	162 (139)	198 (178)	129[f]
Polyethylene			
Cu(111)	102 (100)	145 (136)	···
Cu(100) (a)	118 (114)	160 (146)	120[g]
Cu(100) (b)	118 (114)	155 (145)	120[g]
Cu(110) (a)	121 (114)	160 (147)	···
Cu(110) (b)	119 (112)	155 (144)	···

[a] Reference [34].
[b] Reference [98].
[c] Reference [27].
[d] Reference [35].
[e] Reference [99].
[f] Reference [29].
[g] Reference [28].

TABLE III. Calculated adsorption heights of *n*-butane (polyethylene) on the close-packed metal [low-indexed Cu] surfaces in Å. The rightmost column shows the adsorption heights estimated from the changes in the C–H stretching frequencies and the work functions of polyethylene adsorbed on the metal surfaces.

System	rev-vdW-DF2	optB86b-vdW	Estimates[a]
n-butane			
Cu(111)	3.48	3.45	···
Ag(111)	3.53	3.51	3.90
Au(111)	3.55	3.51	3.52
Ir(111)	3.49	3.45	···
Pt(111)	3.40	3.39	3.56
Ru(0001)	3.49	3.43	3.39
Polyethylene			
Cu(111)	3.49	3.46	···
Cu(100) (a)	3.43	3.37	···
Cu(100) (b)	3.43	3.39	3.83
Cu(110) (a)	3.16, 3.30	3.13, 3.27	···
Cu(110) (b)	3.19, 3.35	3.13, 3.28	···

[a] Reference [52].

adsorption energies are corrected with the ZP energy

$$E_{\mathrm{ZP}} = \sum_i \frac{\hbar\omega_i}{2} \tag{2}$$

with ω_i being the frequency of the i-th molecular vibartion. Note that the ZPC always increases the adsorption energy, which is mainly due to the softening of the C–H bonds pointing towards the surface. The adsorption energy on Cu(111) calculated with optB86b-vdW is in good agreement with the TPD result [34], whereas those on Au(111), Pt(111), and Ru(0001), especially the ZP-corrected values are significantly larger than the experimental ones [27, 29, 34, 35, 98, 99]. In contrast, the calculated adsorption heights on the latter surfaces are close to those estimated from the changes in work functions and C–H stretching frequencies [52]. It should be noted that the adsorption height on Ag(111) is significantly overestimated, which can also be seen in the DFT results obtained with the QUANTUM ESPRESSO code [101] as shown in Sec. III of the Supplementary Material [100]. In addition, the experimental results for Ir(111) are scarce, because *n*-alkanes dissociatively chemisorb on the surface [102]. Our results indicate that rev-vdW-DF2 and optB86-vdW tend to overestimate the adsorption energies of *n*-butane on the close-packed surfaces, whereas exhibit superior performance in the adsorption heights as compared with vdW-DF2 [54], which is known to systematically overestimate equilibrium distances.

2. *Polyethylene adsorbed on low-indexed Cu surfaces*

To see the dependence of the molecule-surface interaction on the facet of a metal surface, we also determine the adsorption structures of polyethylene on the Cu(111), (100), and

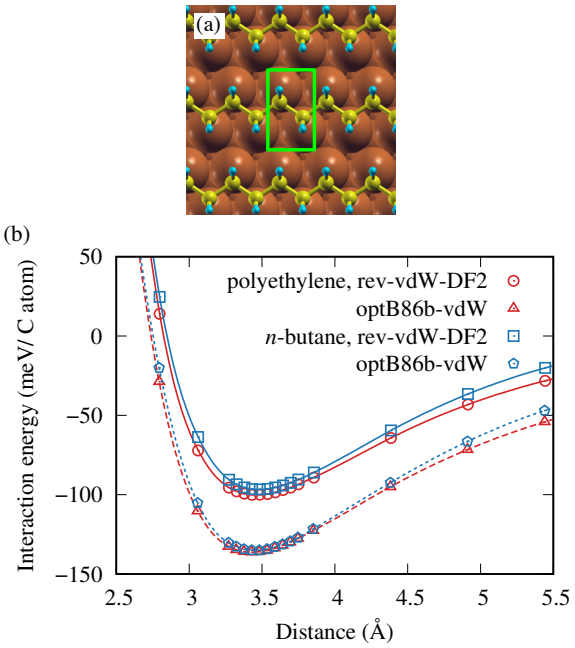

FIG. 3. Schematic views of polyethylene adsorbed on the Cu(111) surface (a), where the rectangle represents the $1\times\sqrt{3}$ unit cell. Panel (b) shows the interaction energies between polyethylene and Cu(111) plotted as a function of the molecule-surface distance. The results for *n*-butane on Cu(111) are also shown for comparison.

(110) surfaces. Note that the length of the repeating unit of polyethylene is close to the nearest neighbor distance of Cu atoms, which is calculated to be 2.56 (2.57) Å with rev-vdW-DF2 (optB86b-vdW). Based on the comparison of the adsorption configurations of *n*-butane on Cu(111) (see Fig. 1), we assume that polyethylene adsorbs on Cu(111) as shown in Fig. 3(a), where C atoms are approximately above the top sites. The interaction energies between polyethylene and Cu(111) are plotted in Fig. 3(b), and the adsorption energies and heights are shown in Tables II and III, respectively. These results are similar to those for *n*-butane on Cu(111), demonstrating that the adsorption of *n*-alkane on metal surfaces little depends on the chain length. Note that the slight deviations in the adsorption energies from those for *n*-butane on Cu(111) reflect the difference in the molecular structures.

The LEED analyses have revealed that polyethylene forms a (1×2) superstructure on Cu(100) with the molecular axis along the [011] or [0$\bar{1}$1] direction [10, 11, 25]. We examine the adsorption configurations as shown in Figs. 4(a)–4(c), where the polyethylene molecule is above a gap between two Cu rows in the former two, while it is just above a Cu row in the latter. The interaction energy between polyethylene and Cu(100) is plotted as a function of the molecule-surface distance in Fig. 4(d). The energy curves for the configurations in Figs. 4(a) and 4(b) almost overlap, suggesting that the displacement of polyethylene along the molecular axis has little influence on the molecule-surface interaction. Moreover, these curves are significantly deeper than that of the configuration in Fig. 4(c). This indicates that polyethylene prefers to adsorb on Cu(100) with the molecular axis above a gap

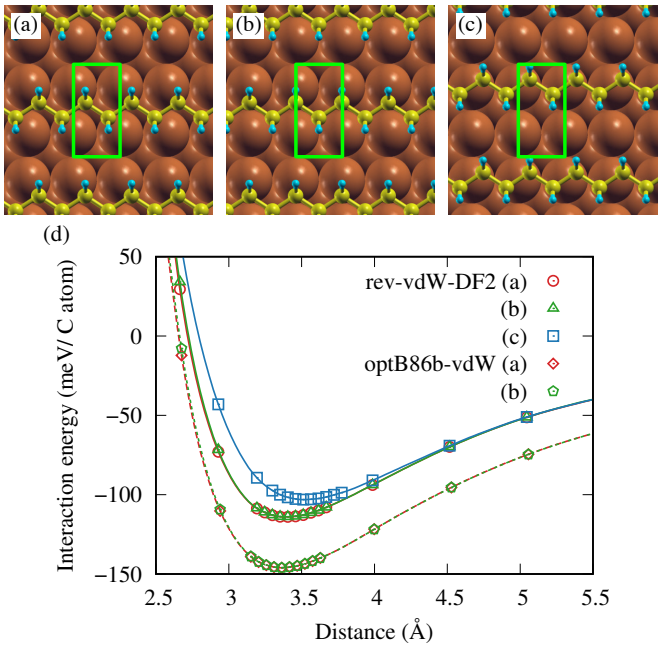

FIG. 4. Schematic views of polyethylene adsorbed on the Cu(100) surface in three different configurations (a)–(c), where the rectangle in each panel represents the (1 × 2) unit cell. Panel (d) shows the interaction energies between polyethylene and Cu(100) plotted as functions of the molecule-surface distance.

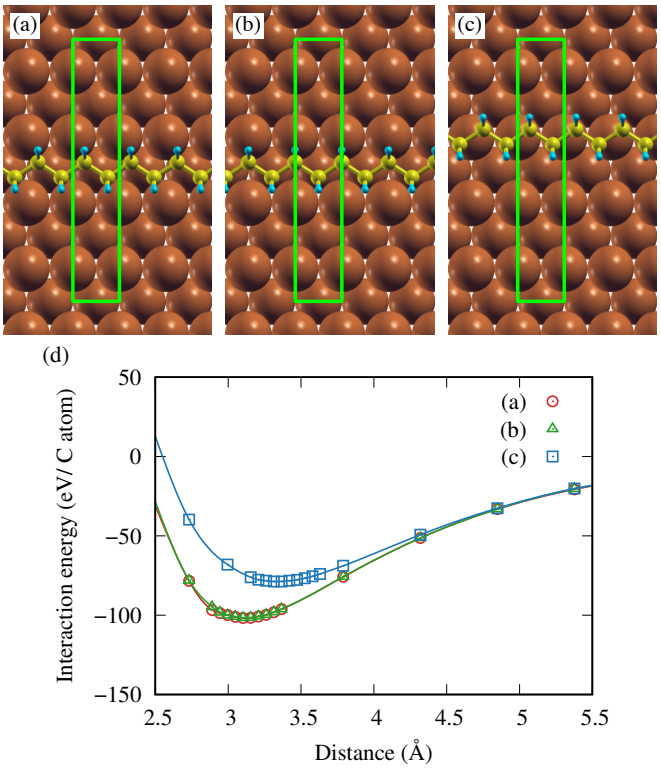

FIG. 5. Schematic views of polyethylene adsorbed on the Cu(110) surface in three different configurations (a)–(c), where one polyethylene molecule is included in the (1 × 4) unit cell represented by the rectangle in each panel. Panel (d) shows the rev-vdW-DF2 results for the interaction energies between polyethylene and Cu(110) plotted as functions of the molecule-surface distance.

between two Cu rows, which remains unchanged even after taking the ZPC into account. As shown in Tables II and III, the adsorption energy calculated with rev-vdW-DF2 is in good agreement with the TPD result [28], whereas the adsorption heights calculated with the two functionals are significantly smaller than the value estimated from the vibrational frequecy and work function [10, 25, 52].

Polyethylene forms a (1×4) superstructure on Cu(110) with the molecular axis along the [1$\bar{1}$0] direction [11], but the details of the superstructure remain unidentified. To determine the adsorption structure of polyethylene on Cu(110), we first examine simple cases in which one polyethylene molecule is included in the (1 × 4) unit cell as shown in Figs 5(a)–5(c), and plot the molecule-surface interaction energies in Fig. 5(d). Parallel to polyethylene on Cu(100) discussed above, the energy curves for the configurations in Figs. 5(a) and 5(b) suggest that the molecule-surface interaction is almost independent of the displacement along the molecular axis, while the comparison with the result for the configuration in Fig. 5(c) indicates that polyethylene prefers to adsorb on a gap between two Cu rows.

We next examine the model proposed in Ref. [11], which includes three polyethylene molecules in the 1 × 4 unit cell. Without the Cu(110) surface, the optimal distance between two polyethylene molecules is close to one-third of the lattice parameter in the [001] direction of the Cu(110)-(1 × 4) unit cell, which are calculated to be 4.73 and 4.84 Å, respectively, with rev-vdW-DF2. We thus focus on the two adsorption configurations shown in Figs. 6(a) and 6(b), where three polyethylene molecules are equally spaced in the [001] direction. In Fig. 6(a) [(b)], one of the three molecules is adsorbed on Cu(110) in the most stable configuration shown in Fig. 5(a) [(b)], while the other two are in a configuration analogous to the metastable one shown in Fig. 5(c). We define the distances of the former and latter polyethylene molecules from the Cu(110) surface as d_1 and d_2, respectively, and plot the molecule-surface interaction energy calculated with rev-vdW-DF2 (optB86b-vdW) as a function of d_1 and d_2 in Figs. 6(d) [6(e)]. These results suggest that there is almost no correlation between d_1 and d_2, and indeed the optimal molecule-surface distances 3.16–3.19 (3.13) and 3.30–3.35 (3.27–3.28) Å for rev-vdW-DF2 (optB86b-vdW) are close to those obtained independently for the configurations in Figs. 5(a) and 5(b), and Fig. 5(c), respectively. Moreover, the average adsorption energy of polyethylene is calculated to be 112–114 meV per C atom with rev-vdW-DF2, which is significantly larger than the depth of the energy curve for the metastable configuration in Fig 5(c). This indicates that the polyethylene molecules are stabilized by the intermolecular interactions, corroborating the 1 × 4 superstructure proposed in Ref. [11].

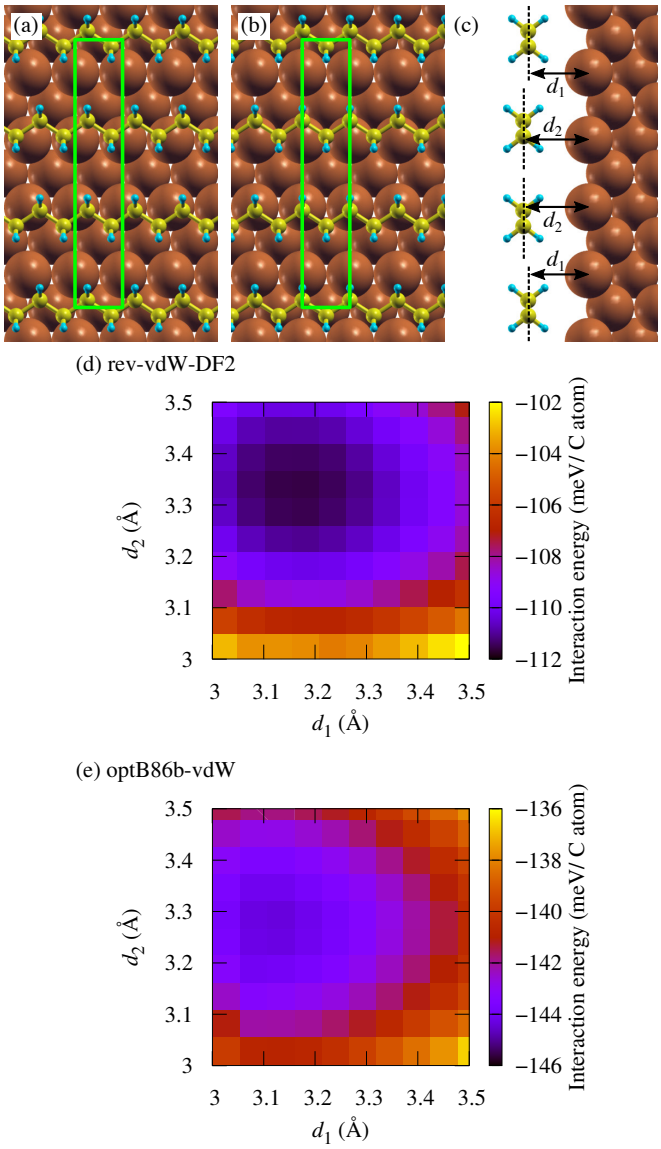

FIG. 6. Top (a)(b) and side (c) views of polyethylene adsorbed on the Cu(110) surface, where three polyethylene molecules are included in the 1×4 unit cell represented by the rectangle in panels (a) and (b). Panels (d) [(e)] shows the rev-vdW-DF2 (optB86b-vdW) results for the interaction energies between polyethylene and Cu(110) plotted as functions of the molecule-surface distances d_1 and d_2 defined in panel (c).

B. Vibrational properties

In the previous section, the influence of molecular vibrations has been included through the ZPC to the adsorption energies. However, the dependence of the ZPC on the molecule-surface distance has not been taken into account, which may affect the accuracy in determining the adsorption structures of *n*-alkane on metal surfaces. Thus we first examine how the ZPC evolves as a function of the molecule-surface distance, taking polyethylene on Cu(100) as an example, because its adsorption height is significantly underestimated by the two

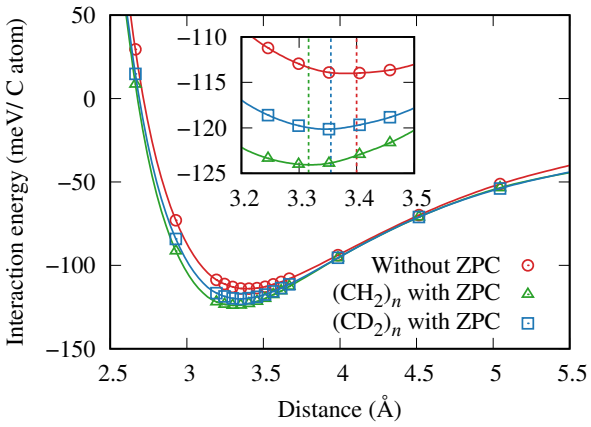

FIG. 7. Interaction energies between polyethylene and Cu(100) with and without ZPC plotted as functions of the molecule-surface distance. The inset shows a zoom-in view near the minimum, where the vertical dashed lines indicate the equilibrium distances. The rev-vdW-DF2 results are shown.

TABLE IV. Calculated C–H stretching frequencies of polyethylene on Cu(100) in cm^{-1}. The results for the adsorption configurations in Figs. 4(a) and 4(b) are shown.

	rev-vdW-DF2		optB86b-vdW	
Mode	Fig. 4(a)	Fig. 4(b)	Fig. 4(a)	Fig. 4(b)
ν_1	2811	2803	2774	2790
ν_2	2824	2819	2801	2828
ν_3	2891	2894	2896	2895
ν_4	2919	2927	2915	2932

vdW functionals as discussed in Sec. III A 2. Fig. 7 shows the molecule-surface interaction energies with and without the ZPC calculated with rev-vdW-DF2 for the adsorption configuration in Fig. 4(a) (See Sec. IV of the Supplementary Material [100] for the analysis of ZPC). The ZP-corrected energy curve for polyethylene on Cu(100) has a deeper minimum at a smaller distance than that without the ZPC, indicating that the adsorption height is further underestimated by including the ZPC. Thus the underestimation of the adsorption height of polyethylene on Cu(100) should be attributed to other reasons. Note that the ZP-corrected curve also deviates from the uncorrected one at large distances, which is due to the influence of intermolecular interactions on the molecular vibrations. Fig. 7 also shows the ZP-corrected interaction energy curve for deuterated polyethylene $(CD_2)_n$ adsorbed on Cu(100), which appears in between the results for the unsubstituted systems with and without the ZPC. The destabilization by replacing atoms with heavier isotopes is referred to as the inverse isotope effect, and has also been observed for cyclohexane on Rh(111) [103, 104]. More recently, the inverse isotopic effect have been theoretically predicted for methane adsorbed on various metal (111) surfaces [105].

The ZP-corrected curves significantly deviate the uncorrected one near the equilibrium distance (Fig. 7), which is due to the changes in the C–H stretching frequencies of polyethy-

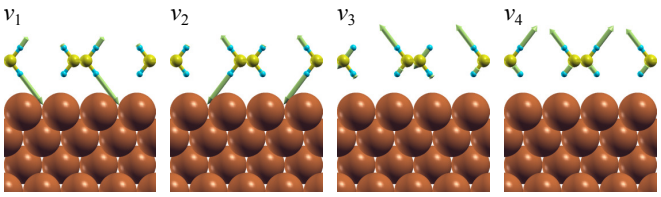

FIG. 8. Schematic views of the C–H stretching modes of polyethylene on Cu(100). The arrows represent the amplitudes and directions of the vibrations of the atoms.

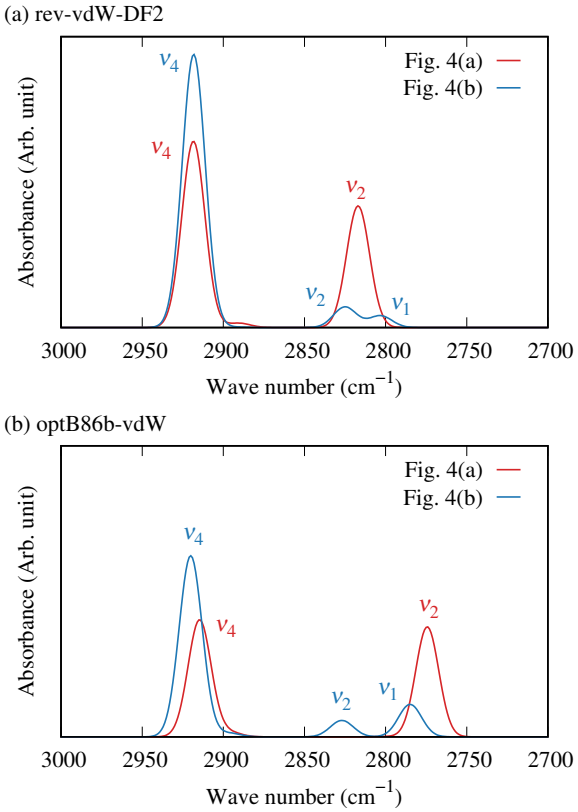

FIG. 9. Absorption spectra of polyethylene on Cu(100) calculated with rev-vdW-DF2 (a) and optB86b-vdW (b). The peaks are smeared by a Gaussian of width 10 cm^{-1}. The results for the adsorption configurations in Figs. 4(a) and 4(b) are shown.

lene upon adsorption on Cu(100). Experimentally, the C–H stretching modes of tetratetracontane (TTC, n-$C_{44}H_{90}$) adsorbed on Cu(100) have been compared with those of crystalline TTC. Namely, IRAS measurements have shown that the ν_s (ν_{as}) mode, which is symmetric (antisymmetric) with respect to the C–C–C plane, appears at 2848 (2918) cm^{-1} for crystalline TTC, while a broad (sharp) peak observed around 2800 (2911) cm^{-1} for TTC on Cu(100) can be assigned to a stretching mode pointing towards the surface (vacuum) [10]. The vibrational frequencies of four C–H stretching modes calculated for polyethylene on Cu(100) are summarized in Table IV. The schematic views of the vibrational modes depicted in Fig. 8 indicate that ν_1 and ν_2 (ν_3 and ν_4) modes

TABLE V. Calculated C–H stretching frequencies of polyethylene on Cu(110) and the vibrational frequencies in cm^{-1}. The results for the adsorption configurations in Figs. 6(a) and 6(b) are shown.

	rev-vdW-DF2		optB86b-vdW	
Mode	Fig. 6(a)	Fig. 6(b)	Fig. 6(a)	Fig. 6(b)
ν_1	2738	2758	2730	2744
ν_2	2766	2786	2758	2771
ν_3	2773	2801	2765	2792
ν_4	2776	2818	2769	2799
ν_5	2832	2855	2832	2834
ν_6	2862	2863	2857	2861
ν_7	2867	2873	2870	2868
ν_8	2883	2892	2883	2880
ν_9	2886	2896	2892	2890
ν_{10}	2893	2901	2895	2892
ν_{11}	2924	2926	2927	2924
ν_{12}	2929	2930	2933	2928

for polyethylene on Cu(100) have larger amplitudes towards the surface (vacuum), but slightly retain a symmetric (antisymmetric) character with respect to the C–C–C plane, and can be related to the ν_s (ν_{as}) mode of crystalline polyethylene, which appears at 2898 (2944) and 2899 (2949) cm^{-1} for rev-vdW-DF2 and optB86b-vdW, respectively. In particular, ν_1 and ν_2 are 74–95 cm^{-1} lower than ν_s for the two adsorption configurations in Figs. 4(a) and (b), which are significantly larger than the experimental value of 48 cm^{-1} [10]. This is consistent with the fact that the vibrational frequencies of these modes decrease monotonically with decreasing the molecule-surface distance [52], and that the adsorption height of polyethylene on Cu(100) is underestimated for the two functionals as discussed in Sec. III A 2. To compare the obtained C–H stretching modes with the experimental results, we calculate the absorption intensity, which is proportional to $(\partial\mu/\partial Q)^2$ with the dipole moment μ of the system and the normal coordinate Q corresponding to a vibrational mode [106]. The calculated absorption spectra are shown in Fig. 9, where the ν_2 and ν_4 modes have comparable peaks for the adsorption configuration in Fig. 4(a), whereas ν_1 and ν_2 modes exhibit much smaller peaks than ν_4 for the adsorption configuration in Fig. 4(b). The latter are more analogous to the broad peak around 2800 cm^{-1} observed experimentally [10]. These results suggest that the adsorption configuration in Fig. 4(b) is more preferable than that in Fig. 4(a), although the relative stabilities of these configurations are indistinguishable based on the adsorption energies.

We also investigate the C–H stretching modes of polyethylene adsorbed on Cu(110). In IRAS measurements, a broad (sharp) peak has been observed at 2760 (2910) cm^{-1} for TTC adsorbed on Cu(110), which are assigned to the C–H stretching modes towards the surface (vacuum) [11]. Table V shows the calculated vibrational frequencies of twelve C–H stretching modes of polyethylene on Cu(110), which is much larger than the number of adsorption peaks observed experimentally.

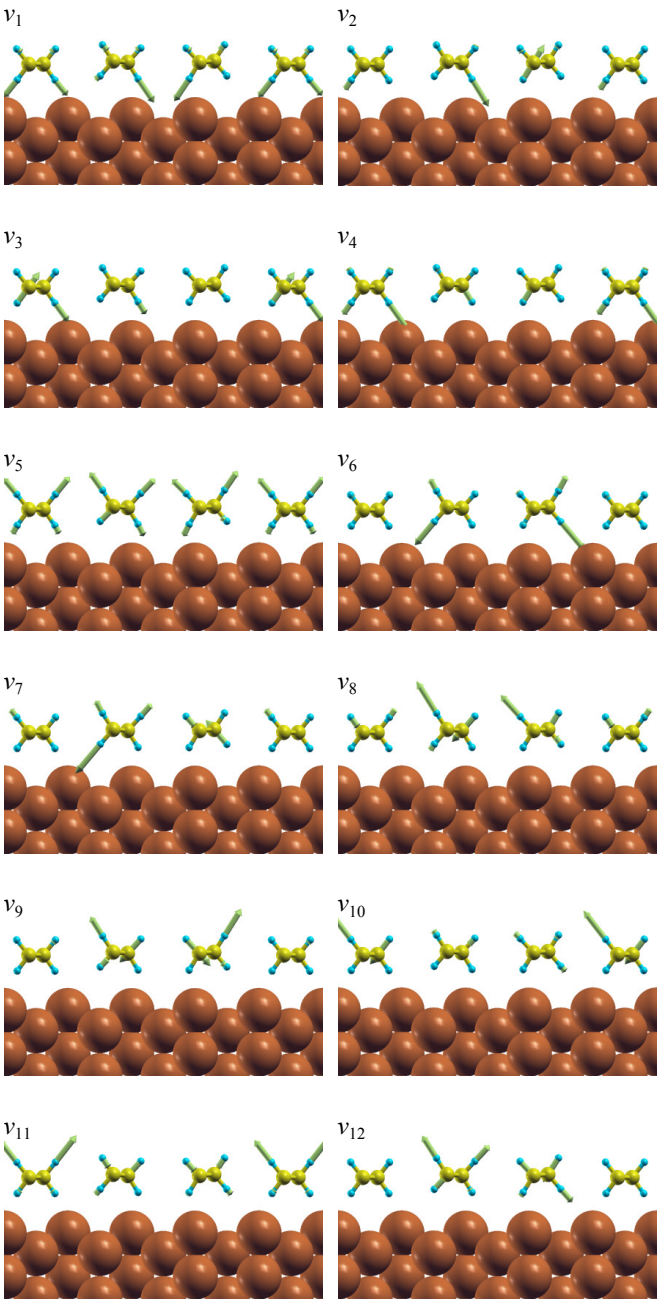

FIG. 10. Schematic views of the C–H stretching modes of polyethylene on Cu(110). The arrows represent the amplitudes and directions of the vibrations of the atoms.

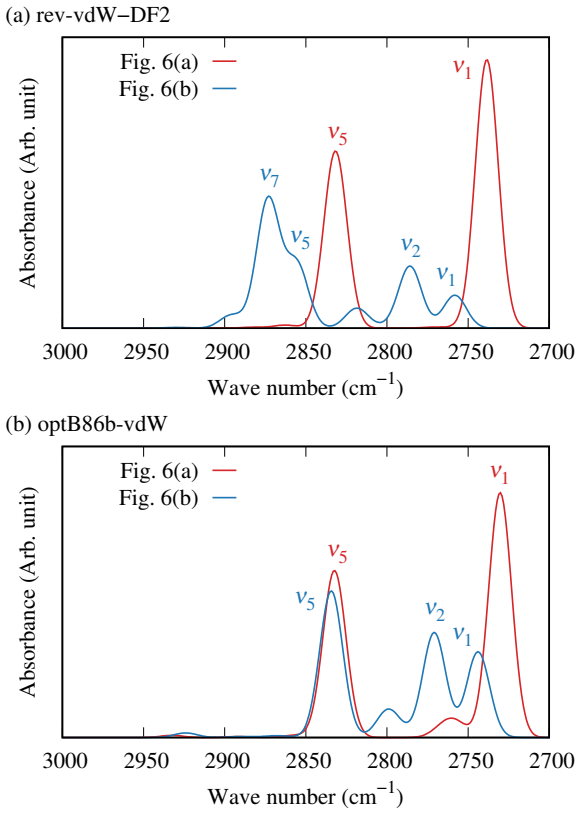

FIG. 11. Absorption spectra of polyethylene on Cu(110) calculated with rev-vdW-DF2 (a) and optB86b-vdW (b). The peaks are smeared by a Gaussian of width 10 cm^{-1}. The results for the adsorption configurations in Figs. 6(a) and 6(b) are shown.

However, the schematic views of the vibrational modes depicted in Fig. 10 indicate that more than half of them are IR-inactive, because of the cancellation of dynamic dipole moments among the three polyethylene molecules. As a consequence, the calculated absorption spectra of the stretching modes are composed of 2–6 peaks as shown in Fig. 11. For the adsorption configuration in Fig. 6(a), the ν_1 mode shows the highest peak at 2730 cm^{-1}. In sharp contrast, the ν_1 and ν_2 modes exhibits smaller peaks for the adsorption configuration in Fig. 6(b), which are more analogous to the broad peak around 2760 cm^{-1} observed experimentally [11], as in the case of polyethylene on Cu(100).

C. Work function

The adsorption of organic molecules on metal surfaces forms dipole layers at the molecule-metal interfaces, which tend to decrease the work functions of the metal surfaces [1]. Thus the changes in the work function upon adsorption also provide useful information about the adsorption structures of *n*-alkanes on metal surfaces. Table VI shows the comparison between the work function changes calculated with vdW-DF and those observed experimentally. To the best of our knowledge, the experimental results are limited to *n*-alkanes on Cu(100) [25], Ag(111) [107], and Au(111) [107, 108], but some trends can be extracted that have been seen above. Namely, the work function changes for Cu(100) and Ag(111) are overestimated by the two vdW functionals, while those for Au(111) are in good agreement with the result observed in Ref. [107], although a recent experiment has reported a larger work function change [108]. These trends are analogous to those seen in the adsorption heights of *n*-alkanes on these surfaces.

To understand the origins of the work function changes ob-

TABLE VI. Calculated work function changes upon adsorption of *n*-alkane on the metal surfaces in eV. The experimental results are obtained for *n*-tetratetracontane adsorbed on the metal surfaces. The values in parentheses are the work functions of clean metal surfaces.

System	rev-vdW-DF2	optB86b-vdW	Experiments[a]
n-butane			
Cu(111)	−0.68 (4.99)	−0.73 (4.98)	··· (4.98)
Ag(111)	−0.71 (4.91)	−0.72 (4.84)	−0.5 ± 0.1[b] (4.74)
Au(111)	−0.62 (5.47)	−0.71 (5.45)	−0.7 ± 0.2[b] (5.31)
			−1[c] (5.31)
Ir(111)	−1.04 (5.76)	−1.09 (5.68)	··· (5.76)
Pt(111)	−1.00 (6.00)	−0.99 (5.94)	··· (5.7)
Ru(0001)	−1.23 (5.60)	−1.28 (5.51)	··· (4.71[d])
Polyethylene			
Cu(111)	−0.85 (4.99)	−0.87 (4.98)	··· (4.98)
Cu(100) (a)	−0.66 (4.72)	−0.69 (4.72)	−0.3[e] (4.59)
Cu(100) (b)	−0.69 (4.72)	−0.69 (4.72)	−0.3[e] (4.59)
Cu(110) (a)	−0.69 (4.66)	−0.74 (4.59)	··· (4.48)
Cu(110) (b)	−0.68 (4.66)	−0.70 (4.59)	··· (4.48)

[a] The values in parentheses are taken from Ref. [109].
[b] Reference [107], polycrystalline.
[c] Reference [108].
[d] Polycrystalline.
[e] Reference [25].

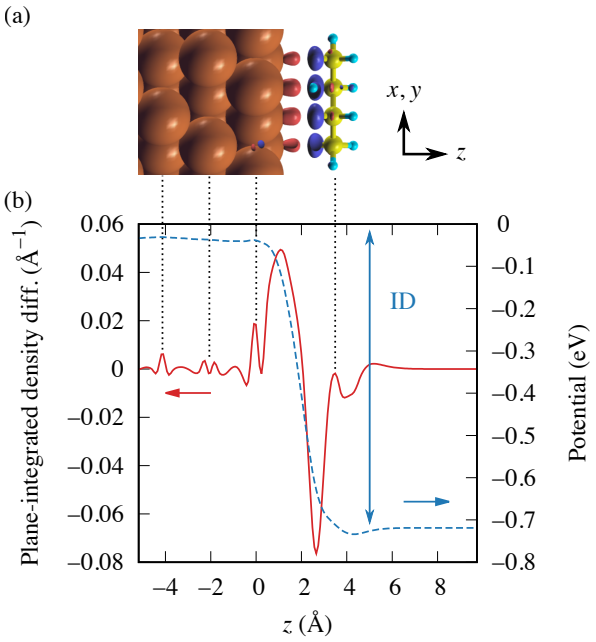

FIG. 12. Electric dipole layer at the interface between *n*-alkane and Cu(111) (a) and plane-integrated electron density difference plotted as a function of the distance from the metal surface (b). Panel (b) also shows the electrostatic potential calculated from the electron density difference. The rev-vdW-DF2 results are shown.

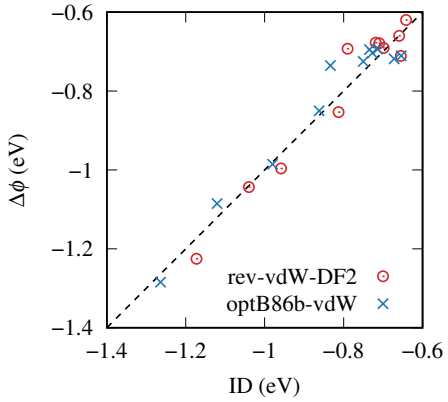

FIG. 13. Comparison between $\Delta\phi$'s and ID's for *n*-alkanes on the metal surfaces.

tained above, we first consider the changes in the electron density upon adsorption of *n*-alkanes on the metal surfaces. Fig. 12(a) shows the rev-vdW-DF2 result for *n*-butane on Cu(111) calculated from the difference between the electron densities before and after the adsorption, with the structures of the molecule and the surface kept fixed to the geometries of the adsorption system. Here the isosurfaces in red (blue) represent increases (decreases) in electron density. We then calculate the electrostatic potential averaged over a plane parallel to the surface $V(z)$ by solving the one-dimensional Poisson equation [110–112]

$$\frac{d^2V}{dz^2} = -\frac{e^2}{\varepsilon_0}\Delta\rho(z), \tag{3}$$

where $\Delta\rho$ denotes the planar average of the electron density difference. e and ε_0 are the elementary charge and the dielectric constant of the vacuum, respectively. The plane-integrated electron density difference as well as $V(z)$ thus obtained are plotted in Fig. 12(b), where ID stands for the potential drop across the interface dipole layer. The results for the other *n*-alkane-metal interfaces are given in Sec. V of the Supplementary Material [100], where the rev-vdW-DF2 and optB86b-vdW results are similar to each other, suggesting that the differences in the adsorption energies and heights obtained with the two functionals in Sec. III A stem from the functional design rather than the electron density distribution. The work function change $\Delta\phi$ upon adsorption of a molecule on a metal surface can be expressed as

$$\Delta\phi = \mathrm{ID} + \Delta V_{\mathrm{mol}} + \Delta V_{\mathrm{surf}}, \tag{4}$$

where ΔV_{mol} (ΔV_{surf}) denotes the potential change due to the distortion of the molecule (surface). The comparison of $\Delta\phi$'s in Table VI and calculated ID's is shown in Fig. 13, which indicates that the work function change is predominantly determined by the formation of interface electric dipoles, hence the adsorption height of *n*-alkane on the metal surface. Although the changes in both the work functions and the C–H stretching frequencies suggest that the two functionals underestimate the adsorption height of *n*-alkanes on Cu(100) and Ag(111), there remains the possibility that the discrepancies are due to the underestimation of the HOMO-LUMO gap inherent to DFT calculations. To gain more insight into the discrepancies, more sophisticated techniques are required such as hybrid function-

als and the random phase approximation (RPA), which has been applied to molecule-metal interfaces [113–115].

IV. CONCLUSION

We have applied vdW-DF to the investigation of the geometrical, vibrational, and electronic properties of *n*-alkanes adsorbed on various metal surfaces. It is found that the rev-vdW-DF2 and optB86b-vdW functionals reproduce the TPD results for the adsorption energies of *n*-alkanes on Cu(100) and Cu(111), respectively, whereas these functionals significantly overestimate those on Au(111), Pt(111), and Ru(0001). In contrast, the adsorption heights of *n*-alkanes on the latter surfaces obtained with these functionals are in good agreement with values estimated from the changes in the work function and the C–H stretching frequencies, whereas those on Cu(100) and Ag(111) are significantly smaller than the estimated values. These results indicate that further improvement of vdW-DF is necessary for the description of *n*-alkanes on metal surfaces with high accuracy.

From the results of the vibrational mode analyses, it is also found that the changes in the C–H stretching frequencies and IRAS spectra are useful for determining the preference of different adsorption structures of similar stability. Recently, an analogous result has been reported for methane adsorbed on Pt(111) [116], where the tripod and monopod configurations have adsorption energies close to each other within the generalized gradient approximation with the many-body dispersion correction [117], whereas the former has a C–H stretching frequency closer to the experimental result than the latter. More importantly, Ref. [116] has also revealed that RPA predicts a clear preference for the tripod configuration. This suggests that RPA enables a better description of *n*-alkanes adsorbed on metal surfaces, which will be discussed elsewhere.

ACKNOWLEDGMENTS

We thank Y. Isozaki and T. Koizumi for providing the results for the adsorption energies and heights calculated with the QUANTUM ESPRESSO code. The present study was supported by Grant-in-Aid for Scientific Research (C) (Grant No. JP21K03419) and by Grant-in-Aid for Fund for the Promotion of Joint International Research (Fostering Joint International Research (B)) (Grant No. JP22KK0071) from the Japan Society for the Promotion of Science (JSPS). The numerical calculations in this work were done using the facilities of Supercomputer Center, Institute for Solid State Physics, University of Tokyo.

[1] H. Ishii, K. Sugiyama, E. Ito, and K. Seki, Energy level alignment and interfacial electronic structures at organic/metal and organic/organic interfaces, Adv. Mater. **11**, 605 (1999).
[2] P. S. Bagus, V. Staemmler, and C. Wöll, Exchangelike effects for closed-shell adsorbates: Interface dipole and work function, Phys. Rev. Lett. **89**, 096104 (2002).
[3] P. S. Bagus, K. Hermann, and C. Wöll, The interaction of C_6H_6 and C_6H_{12} with noble metal surfaces: Electronic level alignment and the origin of the interface dipole, J. Chem. Phys. **123**, 184109 (2005).
[4] M. J. Hostetler, W. L. Manner, R. G. Nuzzo, and G. S. Girolami, Two-dimensional melting transitions of rod-like molecules analyzed by reflection-absorption infrared spectroscopy, J. Phys. Chem. **99**, 15269 (1995).
[5] J. Yoshinobu, H. Ogasawara, and M. Kawai, Symmetry controlled surface photochemistry of methane on Pt(111), Phys. Rev. Lett. **75**, 2176 (1995).
[6] G. Witte, K. Weiss, P. Jakob, J. Braun, K. L. Kostov, and C. Wöll, Damping of molecular motion on a solid substrate: Evidence for electron-hole pair creation, Phys. Rev. Lett. **80**, 121 (1998).
[7] A. Teplyakov, B. Bent, J. Eng, and J. Chen, Vibrational mode-softening of alkanes on clean and modified Cu and Mo surfaces: absence of a simple correlation with thermal desorption temperatures, Surf. Sci. **399**, L342 (1998).
[8] M. Yamamoto, Y. Sakurai, Y. Hosoi, H. Ishii, E. Ito, K. Kajikawa, Y. Ouchi, and K. Seki, Physisorption of a long-chain *n*-alkane on Ag(111) surface: an infra-red reflection absorption spectroscopic study, Surf. Sci. **427-428**, 388 (1999).
[9] M. Yamamoto, Y. Sakurai, Y. Hosoi, H. Ishii, K. Kajikawa, Y. Ouchi, and K. Seki, Softened ch stretching vibration of a long-chain *n*-alkane, *n*-$C_{44}H_{90}$, physisorbed on a Ag(111) surface: An infrared reflection absorption spectroscopic study, J. Phys. Chem. B **104**, 7370 (2000).
[10] Y. Hosoi, Y. Sakurai, M. Yamamoto, H. Ishii, Y. Ouchi, and K. Seki, Structures of a film of the long-chain *n*-alkane *n*-$C_{44}H_{90}$ on a Cu(100) surface, Surf. Sci. **515**, 157 (2002).
[11] Y. Hosoi, Y. Niwa, Y. Sakurai, H. Ishii, Y. Ouchi, and K. Seki, IRRAS and LEED studies of films of the long chain *n*-alkane *n*-$C_{44}H_{90}$ on Cu(100) and Cu(110), Appl. Surf. Sci. **212-213**, 441 (2003).
[12] H. Öström, L. Triguero, K. Weiss, H. Ogasawara, M. G. Garnier, D. Nordlund, M. Nyberg, L. G. M. Pettersson, and A. Nilsson, Orbital rehybridization in *n*-octane adsorbed on Cu(110), J. Chem. Phys. **118**, 3782 (2003).
[13] J. P. Luongo and H. Schonhorn, Infrared study of substrate effects in the surface region of polyethylene, J. Polym. Sci. Part A2 **6**, 1649 (1968).
[14] M. G. Chan and D. L. Allara, Infrared reflection studies of metal-polymer interfaces, Polym. Eng. Sci. **14**, 12 (1974).
[15] L. E. Firment and G. A. Somorjai, Surface structures of normal paraffins and cyclohexane monolayers and thin crystals grown on the (111) crystal face of platinum. A low-energy electron diffraction study, J. Chem. Phys. **66**, 2901 (1977).
[16] S. Sack, S. Schär, E. Steger, and H. Wagner, Studies on the mechanism of the copper-catalyzed thermal oxidation of low-density polyethylene, Polym. Degrad. Stabil. **7**, 193 (1984).
[17] M. Chesters, P. Gardner, and E. McCash, The reflection-absorption infrared spectra of *n*-alkanes adsorbed on Pt(111), Surf. Sci. **209**, 89 (1989).
[18] A. R. Bishop, G. S. Girolami, and R. G. Nuzzo, Structural models and thermal desorption energetics for multilayer assemblies of the *n*-alkanes on Pt(111), J. Phys. Chem. B **104**, 754 (2000).

[19] K. A. Fosser, J. H. Kang, R. G. Nuzzo, and C. Wöll, Adsorption of linear alkanes on Cu(111): Temperature and chain-length dependence of the softened vibrational mode, J. Chem. Phys. **126**, 194707 (2007).

[20] O. Endo, K. Tsuji, and H. Ozaki, Potential-induced reorientation of physisorbed n-hexatriacontane on a Au(111) electrode studied by in-situ infrared reflection absorption spectroscopy, J. Phys. Chem. C **112**, 17336 (2008).

[21] Y. H. Choi, S. E. M. Putra, Y. Shiozawa, S. Tanaka, K. Mukai, I. Hamada, Y. Morikawa, and J. Yoshinobu, The quantitative study of methane adsorption on the Pt(997) step surface as the initial process for reforming reactions, Surf. Sci. **732**, 122284 (2023).

[22] L. E. Firment and G. A. Somorjai, Low-energy electron diffraction study of the surface of thin crystals and monolayers of normal paraffins and cyclohexane on the Ag(111) crystal surface, J. Chem. Phys. **69**, 3940 (1978).

[23] D. Yoshimura, H. Ishii, Y. Ouchi, E. Ito, T. Miyamae, S. Hasegawa, N. Ueno, and K. Seki, Angle-resolved UPS study and simulation with IAC approximation for oriented monolayer of tetratetracontane (n-$C_{44}H_{90}$) on Cu(100), J. Electron Spectrosc. **88-91**, 875 (1998).

[24] D. Fuhrmann, R. Gerlach, H. Rubahn, and C. Wöll, Structure and phase transitions of ultrathin films of alkanes adsorbed on Cu(111), Surf. Sci. **424**, 145 (1999).

[25] D. Yoshimura, H. Ishii, Y. Ouchi, E. Ito, T. Miyamae, S. Hasegawa, K. K. Okudaira, N. Ueno, and K. Seki, Angle-resolved ultraviolet photoelectron spectroscopy and theoretical simulation of a well-ordered ultrathin film of tetratetracontane n-$C_{44}C_{90}$ on Cu(100): Molecular orientation and intramolecular energy-band dispersion, Phys. Rev. B **60**, 9046 (1999).

[26] H. Ishii, E. Morikawa, S. Tang, D. Yoshimura, E. Ito, K. Okudaira, T. Miyamae, S. Hasegawa, P. Sprunger, N. Ueno, K. Seki, and V. Saile, Electronic structure and molecular orientation of well-ordered polyethylene oligomer (n-$C_{44}H_{90}$) on Cu(100) and Au(111) surfaces studied by UV photoemission and low energy electron diffraction, J. Electron Spectrosc. **101-103**, 559 (1999).

[27] J. F. Weaver, M. Ikai, A. Carlsson, and R. J. Madix, Molecular adsorption and growth of n-butane adlayers on Pt(111), Surf. Sci. **470**, 226 (2001).

[28] B. Sexton and A. Hughes, A comparison of weak molecular adsorption of organic molecules on clean copper and platinum surfaces, Surf. Sci. **140**, 227 (1984).

[29] J. L. Brand, M. V. Arena, A. A. Deckert, and S. M. George, Surface diffusion of n-alkanes on Ru(001), J. Chem. Phys. **92**, 5136 (1990).

[30] L. H. Dubois, B. R. Zegarski, and R. G. Nuzzo, Fundamental studies of microscopic wetting on organic surfaces. 2. interaction of secondary adsorbates with chemically textured organic monolayers, J. Am. Chem. Soc. **112**, 570 (1990).

[31] M. McMaster, C. Arumainayagam, and R. Madix, Molecular propane adsorption dynamics on Pt(111), Chem. Phys. **177**, 461 (1993).

[32] M. C. McMaster, S. L. Schroeder, and R. J. Madix, Molecular propane adsorption dynamics on Pt(110)-(1 × 2), Surf. Sci. **297**, 253 (1993).

[33] J. Pawela-Crew and R. J. Madix, Lateral interactions in the desorption kinetics of weakly adsorbed species: unexpected differences in the desorption of C_4 alkenes and alkanes from Ag(110) due to oriented π-bonding of the alkenes, Surf. Sci. **339**, 8 (1995).

[34] R. Z. Lei, A. J. Gellman, and B. Koel, Desorption energies of linear and cyclic alkanes on surfaces: anomalous scaling with length, Surf. Sci. **554**, 125 (2004).

[35] S. L. Tait, Z. Dohnálek, C. T. Campbell, and B. D. Kay, n-alkanes on Pt(111) and on C(0001)/Pt(111): Chain length dependence of kinetic desorption parameters, J. Chem. Phys. **125**, 234308 (2006).

[36] I. Ciobîcă, G. Kramer, Q. Ge, M. Neurock, and R. van Santen, Mechanisms for chain growth in Fischer–Tropsch synthesis over Ru(0001), J. Catal. **212**, 136 (2002).

[37] Z.-P. Liu and P. Hu, A new insight into Fischer–Tropsch synthesis, J. Am. Chem. Soc. **124**, 11568 (2002).

[38] J. M. H. Lo and T. Ziegler, Theoretical studies of the formation and reactivity of C_2 hydrocarbon species on the Fe(100) surface, J. Phys. Chem. C **111**, 13149 (2007).

[39] J. Cheng, X.-Q. Gong, P. Hu, C. M. Lok, P. Ellis, and S. French, A quantitative determination of reaction mechanisms from density functional theory calculations: Fischer–Tropsch synthesis on flat and stepped cobalt surfaces, J. Catal. **254**, 285 (2008).

[40] J. Cheng, P. Hu, P. Ellis, S. French, G. Kelly, and C. M. Lok, A DFT study of the chain growth probability in Fischer–Tropsch synthesis, J. Catal. **257**, 221 (2008).

[41] J. Cheng, P. Hu, P. Ellis, S. French, G. Kelly, and C. M. Lok, Chain growth mechanism in Fischer–Tropsch synthesis: A DFT study of C–C coupling over Ru, Fe, Rh, and Re surfaces, J. Phys. Chem. C **112**, 6082 (2008).

[42] S. G. Shetty, I. M. Ciobîcă, E. J. M. Hensen, and R. A. van Santen, Site regeneration in the Fischer–Tropsch synthesis reaction: a synchronized CO dissociation and C–C coupling pathway, Chem. Commun. **47**, 9822 (2011).

[43] R. van Santen, I. Ciobîcă, E. van Steen, and M. Ghouri, Chapter 3 - Mechanistic issues in Fischer–Tropsch catalysis, in *Advances in Catalysis*, Vol. 54, edited by B. C. Gates and H. Knözinger (Academic Press, 2011) pp. 127–187.

[44] A. Govender, D. Curulla-Ferré, M. Pérez-Jigato, and H. Niemantsverdriet, First-principles elucidation of the surface chemistry of the C_2H_x (x = 0–6) adsorbate series on Fe(100), Molecules **18**, 3806 (2013).

[45] R. Belkada, Y. Shirakawa, M. Kohyama, S. Tanaka, and J. Hidaka, First-principles study of molecule/Al interfaces, Mater. Trans. **47**, 2701 (2006).

[46] M.-L. Yang, Y.-A. Zhu, C. Fan, Z.-J. Sui, D. Chen, and X.-G. Zhou, Density functional study of the chemisorption of C_1, C_2 and C_3 intermediates in propane dissociation on Pt(111), J. Mol. Catal. A: Chem. **321**, 42 (2010).

[47] D. D. Hibbitts, D. W. Flaherty, and E. Iglesia, Effects of chain length on the mechanism and rates of metal-catalyzed hydrogenolysis of n-alkanes, J. Phys. Chem. C **120**, 8125 (2016).

[48] X. Ding, H. Zhu, H. Ren, D. Liu, Z. Yu, N. Shi, and W. Guo, Adsorption and dehydrogenation of C_2–C_6 n-alkanes over a Pt catalyst: a theoretical study on the size effects of alkane molecules and Pt substrates, Phys. Chem. Chem. Phys. **22**, 21835 (2020).

[49] L. Chen, T. D. Huan, Y. C. Quintero, and R. Ramprasad, Charge injection barriers at metal/polyethylene interfaces, J. Mater. Sci. **51**, 506 (2016).

[50] M. Sato, A. Kumada, and K. Hidaka, First-principles studies of carrier injection in polyethylene (PE) and ethylene-vinyl acetate copolymer (EVA) oligomers, IEEE Trans. Dielectr. Electr. Insul. **24**, 574 (2017).

[51] X. Chen, A. Zhao, J. Li, J. Deng, G. Zhang, and X. Zhao, First-principle investigation of the charge injection barriers of polyethylene and polytetrafluoroethylene oligomers, J. Appl.

Phys. **126**, 035101 (2019).
[52] Y. Morikawa, H. Ishii, and K. Seki, Theoretical study of *n*-alkane adsorption on metal surfaces, Phys. Rev. B **69**, 041403(R) (2004).
[53] P. Légaré, P. Moussounda, and M. Haroun, Theoretical simulation of butane isomers adsorption on a Pt(100) surface, Surf. Sci. **600**, 2938 (2006).
[54] K. Lee, Y. Morikawa, and D. C. Langreth, Adsorption of *n*-butane on Cu(100), Cu(111), Au(111), and Pt(111): Van der Waals density-functional study, Phys. Rev. B **82**, 155461 (2010).
[55] L. Nykänen and K. Honkala, Density functional theory study on propane and propene adsorption on Pt(111) and PtSn alloy surfaces, J. Phys. Chem. C **115**, 9578 (2011).
[56] S. Gautier, S. N. Steinmann, C. Michel, P. Fleurat-Lessard, and P. Sautet, Molecular adsorption at Pt(111). How accurate are DFT functionals?, Phys. Chem. Chem. Phys. **17**, 28921 (2015).
[57] M. Dion, H. Rydberg, E. Schröder, D. C. Langreth, and B. I. Lundqvist, Van der waals density functional for general geometries, Phys. Rev. Lett. **92**, 246401 (2004).
[58] S. Grimme, Accurate description of van der Waals complexes by density functional theory including empirical corrections, J. Comput. Chem. **25**, 1463 (2004).
[59] S. Grimme, Semiempirical GGA-type density functional constructed with a long-range dispersion correction, J. Comput. Chem. **27**, 1787 (2006).
[60] S. Grimme, J. Antony, S. Ehrlich, and H. Krieg, A consistent and accurate *ab initio* parametrization of density functional dispersion correction (DFT-D) for the 94 elements H-Pu, J. Chem. Phys. **132**, 154104 (2010).
[61] A. Tkatchenko and M. Scheffler, Accurate molecular van der Waals interactions from ground-state electron density and free-atom reference data, Phys. Rev. Lett. **102**, 073005 (2009).
[62] A. Tkatchenko, R. A. DiStasio, R. Car, and M. Scheffler, Accurate and efficient method for many-body van der Waals interactions, Phys. Rev. Lett. **108**, 236402 (2012).
[63] T. Thonhauser, V. R. Cooper, S. Li, A. Puzder, P. Hyldgaard, and D. C. Langreth, Van der waals density functional: Self-consistent potential and the nature of the van der Waals bond, Phys. Rev. B **76**, 125112 (2007).
[64] T. Thonhauser, S. Zuluaga, C. A. Arter, K. Berland, E. Schröder, and P. Hyldgaard, Spin signature of nonlocal correlation binding in metal-organic frameworks, Phys. Rev. Lett. **115**, 136402 (2015).
[65] O. A. Vydrov and T. Van Voorhis, Nonlocal van der Waals density functional made simple, Phys. Rev. Lett. **103**, 063004 (2009).
[66] O. A. Vydrov and T. Van Voorhis, Implementation and assessment of a simple nonlocal van der Waals density functional, J. Chem. Phys. **132**, 164113 (2010).
[67] O. A. Vydrov and T. Van Voorhis, Nonlocal van der Waals density functional: The simpler the better, J. Chem. Phys. **133**, 244103 (2010).
[68] K. Lee, E. D. Murray, L. Kong, B. I. Lundqvist, and D. C. Langreth, Higher-accuracy van der Waals density functional, Phys. Rev. B **82**, 081101(R) (2010).
[69] J. Klimeš, D. R. Bowler, and A. Michaelides, Van der Waals density functionals applied to solids, Phys. Rev. B **83**, 195131 (2011).
[70] R. Sabatini, T. Gorni, and S. de Gironcoli, Nonlocal van der Waals density functional made simple and efficient, Phys. Rev. B **87**, 041108(R) (2013).
[71] I. Hamada, van der Waals density functional made accurate, Phys. Rev. B **89**, 121103(R) (2014).
[72] K. Berland and P. Hyldgaard, Exchange functional that tests the robustness of the plasmon description of the van der Waals density functional, Phys. Rev. B **89**, 035412 (2014).
[73] D. Chakraborty, K. Berland, and T. Thonhauser, Next-generation nonlocal van der waals density functional, J.Chem. Theory Comput. **16**, 5893 (2020).
[74] V. Shukla, Y. Jiao, C. M. Frostenson, and P. Hyldgaard, vdW-DF-ahcx: a range-separated van der Waals density functional hybrid, J. Phys.: Condens. Matter **34**, 025902 (2021).
[75] V. Shukla, Y. Jiao, J.-H. Lee, E. Schröder, J. B. Neaton, and P. Hyldgaard, Accurate nonempirical range-separated hybrid van der waals density functional for complex molecular problems, solids, and surfaces, Phys. Rev. X **12**, 041003 (2022).
[76] M. Callsen and I. Hamada, Assessing the accuracy of the van der Waals density functionals for rare-gas and small molecular systems, Phys. Rev. B **91**, 195103 (2015).
[77] Y. Morikawa, K. Iwata, and K. Terakura, Theoretical study of hydrogenation process of formate on clean and Zn deposited Cu(111) surfaces, Appl. Surf. Sci. **169-170**, 11 (2001).
[78] STATE. `https://state-doc.readthedocs.io` (accessed Feb. 22, 2024).
[79] D. Vanderbilt, Soft self-consistent pseudopotentials in a generalized eigenvalue formalism, Phys. Rev. B **41**, 7892 (1990).
[80] N. Troullier and J. L. Martins, Efficient pseudopotentials for plane-wave calculations, Phys. Rev. B **43**, 1993 (1991).
[81] G. Román-Pérez and J. M. Soler, Efficient implementation of a van der Waals density functional: Application to double-wall carbon nanotubes, Phys. Rev. Lett. **103**, 096102 (2009).
[82] J. Wu and F. Gygi, A simplified implementation of van der Waals density functionals for first-principles molecular dynamics applications, J. Chem. Phys. **136**, 224107 (2012).
[83] Y. Hamamoto, I. Hamada, K. Inagaki, and Y. Morikawa, Self-consistent van der Waals density functional study of benzene adsorption on Si(100), Phys. Rev. B **93**, 245440 (2016).
[84] D. C. Langreth and S. Vosko, Response functions and nonlocal approximations, in *Advances in Quantum Chemistry*, Vol. 21 (Elsevier, 1990) pp. 175–199.
[85] J. Schwinger, Thomas-Fermi model: The leading correction, Phys. Rev. A **22**, 1827 (1980).
[86] J. Schwinger, Thomas-Fermi model: The second correction, Phys. Rev. A **24**, 2353 (1981).
[87] K. Berland, D. Chakraborty, and T. Thonhauser, van der Waals density functional with corrected C_6 coefficients, Phys. Rev. B **99**, 195418 (2019).
[88] A. D. Becke, On the large-gradient behavior of the density functional exchange energy, J. Chem. Phys. **85**, 7184 (1986).
[89] B. Vlaisavljevich, J. Huck, Z. Hulvey, K. Lee, J. A. Mason, J. B. Neaton, J. R. Long, C. M. Brown, D. Alfè, A. Michaelides, *et al.*, Performance of van der Waals corrected functionals for guest adsorption in the M_2(dobdc) metal–organic frameworks, J. Phys. Chem. A **121**, 4139 (2017).
[90] I. Cabria, M. López, and J. Alonso, Searching for DFT-based methods that include dispersion interactions to calculate the physisorption of H_2 on benzene and graphene, J. Chem. Phys. **146**, 214104 (2017).
[91] J. G. Brandenburg, A. Zen, D. Alfè, and A. Michaelides, Interaction between water and carbon nanostructures: How good are current density functional approximations?, J. Chem. Phys. **151**, 214104 (2019).
[92] Y. Wong, Y. H. Choi, S. Tanaka, H. Yoshioka, K. Mukai, H. H. Halim, A. R. Mohamed, K. Inagaki, Y. Hamamoto, I. Hamada, *et al.*, Adsorption of CO_2 on terrace, step, and defect sites on

Pt surfaces: a combined TPD, XPS, and DFT study, J Phys. Chem. C **125**, 23657 (2021).
[93] M. Fischer and J. Brauer, Studying the adsorption of emerging organic contaminants in zeolites with dispersion-corrected density functional theory calculations: From numbers to recommendations, ChemistryOpen , e202300273 (2022).
[94] R. W. G. Wyckoff, *Crystal Structures* (Interscience, New York, 1963).
[95] See, e.g., E. B. Wilson, Jr., J. C. Decius, P. C. Cross, *Molecular Vibrations: The Theory of Infrared and Raman Vibrational Spectra* (McGraw-Hill Inc., New York, 1955).
[96] M. Otani and O. Sugino, First-principles calculations of charged surfaces and interfaces: A plane-wave nonrepeated slab approach, Phys. Rev. B **73**, 115407 (2006).
[97] I. Hamada, M. Otani, O. Sugino, and Y. Morikawa, Green's function method for elimination of the spurious multipole interaction in the surface/interface slab model, Phys. Rev. B **80**, 165411 (2009).
[98] S. M. Wetterer, D. J. Lavrich, T. Cummings, S. L. Bernasek, and G. Scoles, Energetics and kinetics of the physisorption of hydrocarbons on Au(111), J. Phys. Chem. B **102**, 9266 (1998).
[99] J. F. Weaver, A. F. Carlsson, and R. J. Madix, The adsorption and reaction of low molecular weight alkanes on metallic single crystal surfaces, Surf. Sci. Rep. **50**, 107 (2003).
[100] See Supplementary Material at http://xxx, which includes Ref. [118], for the adsorption energies and heights calculated with QUANTUM ESPRESSO, the analyses of the ZP-correction, and the interface dipoles calculated for various metal surfaces.
[101] P. Giannozzi, S. Baroni, N. Bonini, M. Calandra, R. Car, C. Cavazzoni, D. Ceresoli, G. L. Chiarotti, M. Cococcioni, I. Dabo, A. D. Corso, S. de Gironcoli, S. Fabris, G. Fratesi, R. Gebauer, U. Gerstmann, C. Gougoussis, A. Kokalj, M. Lazzeri, L. Martin-Samos, N. Marzari, F. Mauri, R. Mazzarello, S. Paolini, A. Pasquarello, L. Paulatto, C. Sbraccia, S. Scandolo, G. Sclauzero, A. P. Seitsonen, A. Smogunov, P. Umari, and R. M. Wentzcovitch, Quantum espresso: a modular and open-source software project for quantum simulations of materials, J. Phys.: Condens. Matter **21**, 395502 (2009).
[102] D. F. Johnson and W. H. Weinberg, Quantification of the selective activation of C–H bonds in short chain alkanes: The reactivity of ethane, propane, isobutane, *n*-butane, and neopentane on Ir(111), J. Chem. Phys. **103**, 5833 (1995).
[103] T. Koitaya, S. Shimizu, K. Mukai, S. Yoshimoto, and J. Yoshinobu, Kinetic and geometric isotope effects originating from different adsorption potential energy surfaces: Cyclohexane on Rh(111), J. Chem. Phys. **136**, 214705 (2012).
[104] K. Fidanyan, I. Hamada, and M. Rossi, Quantum nuclei at weakly bonded interfaces: The case of cyclohexane on Rh(111), Adv. Theory Simul. **4**, 2000241 (2021).
[105] S. E. M. Putra, Y. Morikawa, and I. Hamada, Isotope effect of methane adsorbed on fcc metal (111) surfaces, Chem. Phys. Lett. **780**, 138943 (2021).
[106] Y. Chabal, Surface infrared spectroscopy, Surf. Sci. Rep. **8**, 211 (1988).
[107] E. Ito, H. Oji, H. Ishii, K. Oichi, Y. Ouchi, and K. Seki, Interfacial electronic structure of long-chain alkane/metal systems studied by UV-photoelectron and metastable atom electron spectroscopies, Chem. Phys. Lett. **287**, 137 (1998).
[108] H. Mizushima, H. Koike, K. Kuroda, Y. Ishida, M. Nakayama, K. Mase, T. Kondo, S. Shin, and K. Kanai, Effect of physisorption of inert organic molecules on Au(111) surface electronic states, Phys. Chem. Chem. Phys. **19**, 18646 (2017).
[109] H. B. Michaelson, The work function of the elements and its periodicity, J. Appl. Phys. **48**, 4729 (1977).
[110] G. Heimel, L. Romaner, J.-L. Brédas, and E. Zojer, Interface energetics and level alignment at covalent metal-molecule junctions: π-conjugated thiols on gold, Phys. Rev. Lett. **96**, 196806 (2006).
[111] G. Heimel, L. Romaner, E. Zojer, and J.-L. Brédas, Toward control of the metal-organic interfacial electronic structure in molecular electronics: A first-principles study on self-assembled monolayers of π-conjugated molecules on noble metals, Nano Lett. **7**, 932 (2007).
[112] L. Romaner, G. Heimel, J.-L. Brédas, A. Gerlach, F. Schreiber, R. L. Johnson, J. Zegenhagen, S. Duhm, N. Koch, and E. Zojer, Impact of bidirectional charge transfer and molecular distortions on the electronic structure of a metal-organic interface, Phys. Rev. Lett. **99**, 256801 (2007).
[113] L. Schimka, J. Harl, A. Stroppa, A. Grüneis, M. Marsman, F. Mittendorfer, and G. Kresse, Accurate surface and adsorption energies from many-body perturbation theory, Nat. Mater. **9**, 741 (2010).
[114] Z. Wei, F. Göltl, and P. Sautet, Diffusion barriers for carbon monoxide on the Cu(001) surface using many-body perturbation theory and various density functionals, J. Chem. Theory Comput. **17**, 7862 (2021).
[115] N. A. Szaro, M. Bello, C. H. Fricke, O. H. Bamidele, and A. Heyden, Benchmarking the accuracy of density functional theory against the random phase approximation for the ethane dehydrogenation network on Pt(111), J. Phys. Chem. Lett. **14**, 10769 (2023).
[116] C. Sheldon, J. Paier, and J. Sauer, Adsorption of CH_4 on the Pt(111) surface: Random phase approximation compared to density functional theory, J. Chem. Phys. **155**, 174702 (2021).
[117] A. Ambrosetti, A. M. Reilly, J. DiStasio, Robert A., and A. Tkatchenko, Long-range correlation energy calculated from coupled atomic response functions, J. Chem. Phys. **140**, 18A508 (2014).
[118] G. Kresse and D. Joubert, From ultrasoft pseudopotentials to the projector augmented-wave method, Phys. Rev. B **59**, 1758 (1999).